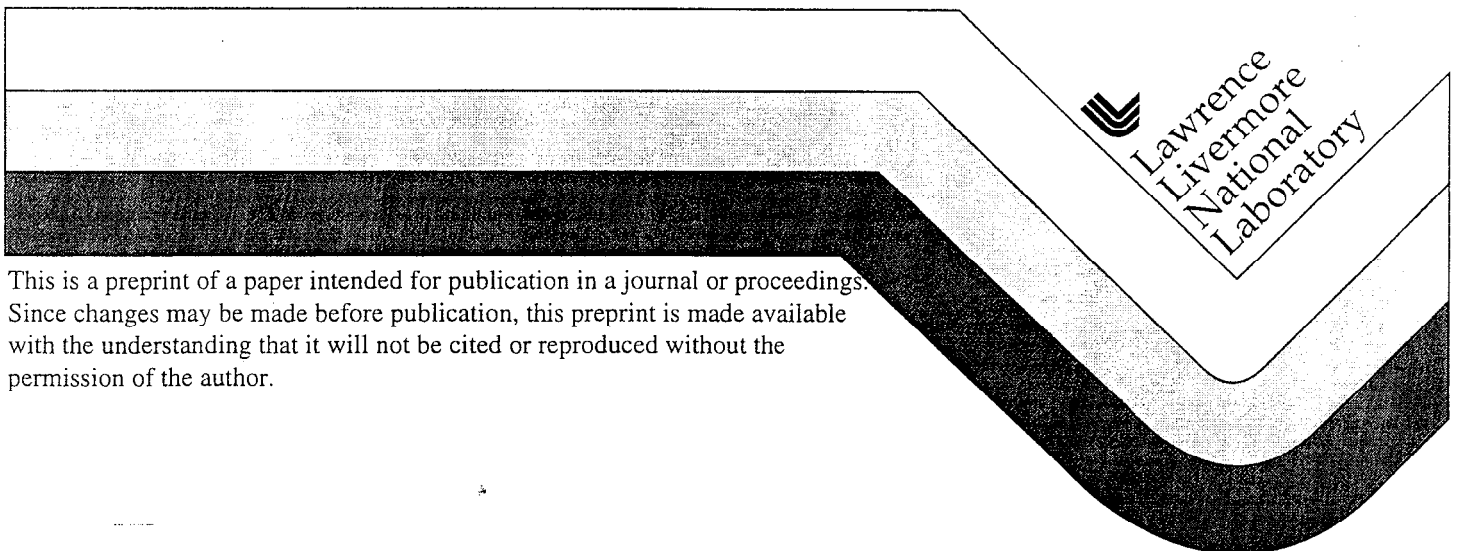


Fluid Flow in 0.5-m Scale Blocks of Topopah Spring Tuff

M.S. Costantino
S. C. Blair
S. R. Carlson

This paper was prepared for submittal to
37th U.S. Rock Mechanics Symposium
Vail, CO
June 6-9, 1999

February 1, 1999



DISCLAIMER

This document was prepared as an account of work sponsored by an agency of the United States Government. Neither the United States Government nor the University of California nor any of their employees, makes any warranty, express or implied, or assumes any legal liability or responsibility for the accuracy, completeness, or usefulness of any information, apparatus, product, or process disclosed, or represents that its use would not infringe privately owned rights. Reference herein to any specific commercial product, process, or service by trade name, trademark, manufacturer, or otherwise, does not necessarily constitute or imply its endorsement, recommendation, or favoring by the United States Government or the University of California. The views and opinions of authors expressed herein do not necessarily state or reflect those of the United States Government or the University of California, and shall not be used for advertising or product endorsement purposes.

Fluid flow in 0.5-m scale blocks of Topopah Spring tuff

M.S. Costantino, S.C. Blair, and S.R. Carlson

Lawrence Livermore National Laboratory, Livermore, California

ABSTRACT: A laboratory experiment was conducted on a 0.5-m scale block of Topopah Spring tuff, to measure fluid flow and mechanical deformation properties under conditions that approximate the near-field environment of a potential nuclear waste repository, and to provide an intermediate-scale test case for numerical model validation. The test specimen is a $0.25 \times 0.25 \times 0.50$ m rectangular prism bisected by an artificial (saw-cut) fracture orthogonal to the tuff fabric. Water was supplied by a point source at the center of the fracture under various pressures of up to 0.04 MPa. Both fluid flow and mechanical properties were found to be anisotropic and strongly correlated with the ash flow fabric. Fluid mass-balance measurements revealed that only minor imbibition of water occurred through the fracture surfaces and that flow rates were independent of normal stress to 14.0 MPa and temperature to 140°C. Flow through the fracture occurred largely through uncorrelated porosity that intersected the fracture plane.

1 INTRODUCTION

The hydrologic response of fluids in the proposed nuclear waste repository horizon at Yucca Mountain (YM) is a critical factor in the repository design. Recent analysis of hydrologic data implies that the rate of water infiltration into YM rock may have been as much as 30 mm/yr, although estimates for the present flux range between 5 and 15 mm/yr (Taylor 1997). Because the repository horizon contains a significant number of fractures, water transport in the YM hydrologic model is dominated by episodic fast flow in fractures (Nitao et al. 1993, Taylor 1997). The amount of water that reaches the repository horizon also depends on imbibition into the host rock through the fracture surfaces, and recent discussion (Hardin et al. 1998) indicates that imbibition values currently used in many hydrologic models must be re-assessed. Moreover, results from the Large Block Test (LBT) (Lin et al. 1995) at Fran Ridge near YM indicate that thermal regimes in partially saturated fractured rock can be dramatically perturbed by small fluctuations in water infiltration rates or by small changes in thermal and mechanical boundary conditions, including temperature excursions and rock-mass displacements not currently accounted for in thermal-hydrologic-mechanical (THM) models of the potential repository. The thermal field and the permeability of the fracture network in the near-field environment (NFE) clearly dominate seepage into the repository. The thermal

field itself is perturbed significantly by “heat pipes” formed by fluid in fractures and connected porosity. Further, the sum of the thermally induced stresses and the relaxation stresses owing to the drift excavation determines the rock-mass stability.

Experiments on intermediate-scale (0.5-m) samples contribute to the understanding of these phenomena, especially flow in discrete fractures under well-characterized thermal and mean stress fields. Results of these experiments provide phenomenological data on the fluid flow in fractured rocks at the characteristic temperature and stress conditions of the NFE. In addition, they contribute to the quantitative physical parameter database used in simulations of the potential repository. Finally and most importantly, they provide laboratory-controlled cases with known boundary and initial conditions for computer-model validation tests. In contrast to centimeter-scale samples, heterogeneities such as porosity, vugs, and healed fractures can be treated stochastically. Introduction of a single, well-characterized fracture provides an ideal test case for the physics required in discrete fracture and dual continuum models.

The work presented here is a continuation of experiments on small-block samples (Blair & Berge 1996, Blair & Costantino 1997). Those reports documented the first of a series of four experiments designed to study coupled processes in the NFE of a nuclear waste repository, and they provided new deformation, elastic-wave-velocity, thermal, and fluid-

flow data that permit approximation of total rock-mass properties and behavior for welded tuff units that contain fractures and vugs. They also provided guidance for material parameters used in various equivalent continuum models of a repository. We report here results of a fracture-flow experiment on a 0.5-m scale block of Topopah Spring tuff, consisting of fluid-flow measurements at stresses of $0.1 \text{ MPa} \leq \sigma_1 \leq 14 \text{ MPa}$ normal to a horizontal fracture, at temperatures in the range $20^\circ\text{C} \leq T \leq 140^\circ\text{C}$. The data and discussion included in this report have been summarized (Blair & Costantino 1997) and reported in depth (Costantino et al. 1998).

2 EXPERIMENT

The sample is a $26.2 \times 24.5 \times 49.0 \text{ cm}$ block cut from a boulder of Topopah Spring tuff excavated at the LBT site. The rock exhibits the typical Topopah Spring tuff fabric of pink, subparallel vugs and gray, densely welded tuff. The block surfaces were cut parallel to the vug axes, and the block was then bisected at the midplane to form an artificial fracture. The fracture surfaces were ground parallel to within 0.025 mm , then roughened using a beadblaster and $100\text{-}\mu\text{m}$ silicon-dioxide beads. About 6 mm of material was removed from the fracture surfaces during cutting and grinding operations, after which the blocks were exposed to the ambient laboratory environment with no special temperature or humidity controls. Although the initial saturation is unknown, calculations using sample weight, dimensions, and a grain density of 2.55 g/cm^3 yield a porosity of 10% , typical for Topopah Spring tuff. Visual inspection of the sample surfaces reveals numerous elongated pores, a few mm wide and a few tens of mm long. Surface roughness was measured at 0.5- and

0.05-mm intervals over portions of one fracture plane with a contacting stylus profilometer developed by Keller and Bonner (1985). The surface profiles show a series of broad mesa-like features, separated by depressions $2\text{--}4 \text{ mm}$ wide and $0.5\text{--}3.0 \text{ mm}$ deep. A typical surface profile, with great vertical exaggeration, is given in Figure 1.

Sixteen linear voltage displacement transducers (LVDTs) were mounted along the vertical surfaces of the blocks. The LVDTs measured axial displacements over four baselines that almost span the entire length of the blocks, four short baselines that cross the fracture plane, and other baselines that span either typical tuff matrix or a major vug. Twelve Type J thermocouples were mounted in 3-mm -diameter holes arranged in a cross pattern along the south face of the sample. The thermocouples were grouted in place, for mechanical stability and to prevent fluid flow through the thermocouple holes.

The fluid-flow system consisted of a pressurized reservoir, a point source in the lower block at the center of the fracture plane, and a collection manifold of 40 evenly-spaced ports, each about 20 mm long, along the fracture perimeter. Fluid pressure of up to 6 psi was controlled to within $\pm 0.1 \text{ psi}$ using a regulator and laboratory compressed air. The fluid passing through the manifold ports was collected in glass jars and weighed at regular intervals.

Temperatures are accurate to $\pm 2.2^\circ\text{C}$ and precise to better than $\pm 0.5^\circ\text{C}$. Precision of the LVDT data was limited by the resolution of the A/D card to about 0.013 mm . Mean axial stress normal to the fracture was found by measuring total axial force with a calibrated load cell with $\pm 0.3\%$ precision, then dividing by the cross-sectional area of the block at 0.1 MPa . Fluid pressures were measured to about $\pm 0.1 \text{ psi}$ with a Bourdon pressure gauge, and volumes were found by dividing water mass by density.

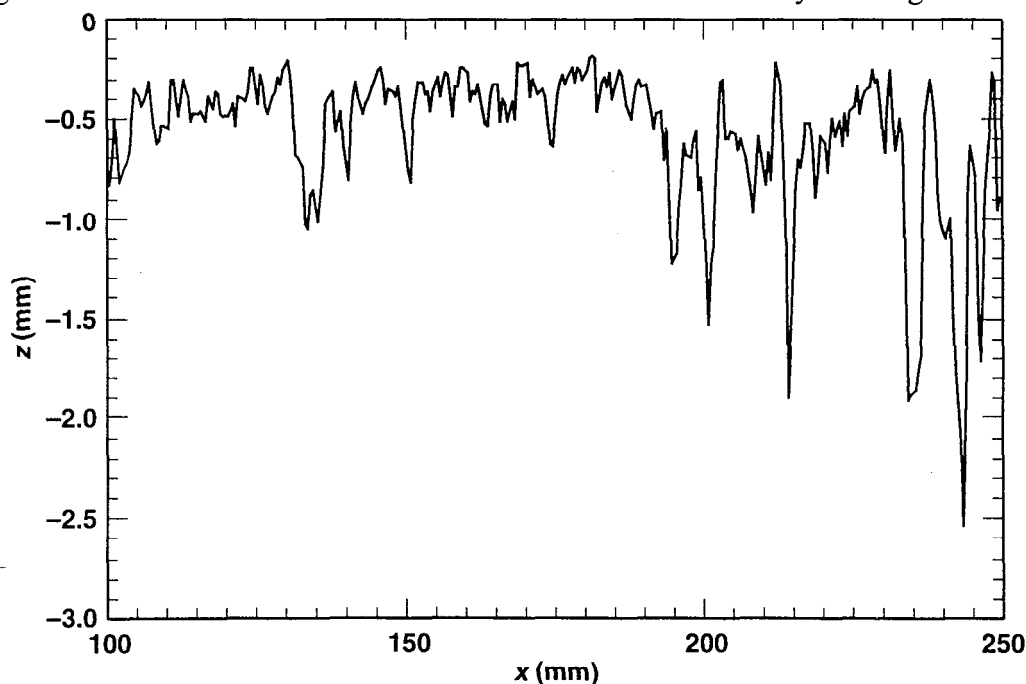


Figure 1. Representative surface topography profile

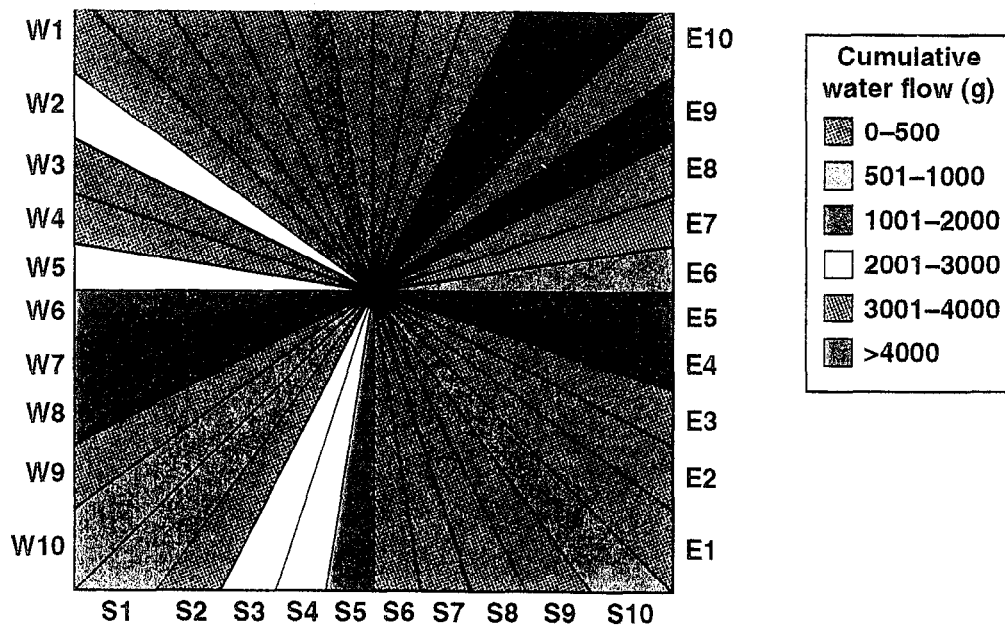


Figure 2. Directional distribution of fluid flow in the fracture plane

Uniaxial stress was applied normal to the fracture plane with a 300-ton press. The sample assembly was heated with point-source heaters attached to copper plates at the top and bottom of the assembly and, for tests above 100°C, on the sample sides. The experiment plan was to measure strains and fluid flow rates as a function of axial stress, temperature and fluid pressure. The test matrix consists of five nominal temperatures (20°, 50°, 75°, 110°, and 140°C), nine axial stresses (0, 1, 2, 4, 6, 8, 10, 12, and 14 MPa), and five pressures (2, 3, 4, 5, and 6 psi). Water flow was measured under each set of conditions until steady state flow was achieved, usually within 3 hours.

3 RESULTS

3.1 Directional flow

The use of a grid of fluid-collection ports with spatial resolution greater than the typical hydrologic network path permits semi-quantitative analysis of flow at the sample boundary. All but a small fraction of the water was collected through 15 ports, with a mere five ports dominating the flow (Figure 2). The major flow paths were in the center of each face and were oriented in the laboratory east-west and north-south directions. The flow pattern correlates well with the surface topography, which is dominated by east-west oriented elongated pores and vugs.

3.2 Fluid flow versus differential pressure

Fluid flux into the fracture can be partitioned into the flux into the initially unsaturated rock through the fracture surfaces and the flux out of the fracture through the collection manifold. Dry rock in contact with a fully saturated boundary, such as a fluid-filled fracture, imbibes water according to Richards' equation, which has a solution with a weak, long-term flow proportional to time t and a stronger, short-term flow proportional to $t^{1/2}$ (Richards 1931). Although we did not measure the short-term transient directly, Figure 3 shows that approximately 110 g of water was imbibed into the dry, porous rock along the fracture plane. The transient flux lasted less than 30 minutes, after which the fluid flux into and out of the fracture was linear in time.

The water mass-balance results for all tests are summarized in Figure 4. For each, cumulative water mass flow into the fracture and out of the collection manifold is plotted against time to find mass flow rate. The flow rates are then plotted against differential pressure to provide an estimate of the mean fracture hydraulic conductivity. Comparison of the slopes of the water input and output curves for each test also provides an estimate for the coefficient of the linear term in time in Richards' equation.

3.3 Fluid flow versus axial stress

Axial stresses to 14 MPa, an upper bound for Yucca Mountain, caused the average fracture aperture to close by about 0.04 cm. Surprisingly, water flow rates were found to be independent of fracture aperture, as parameterized by axial stress (Figure 5).

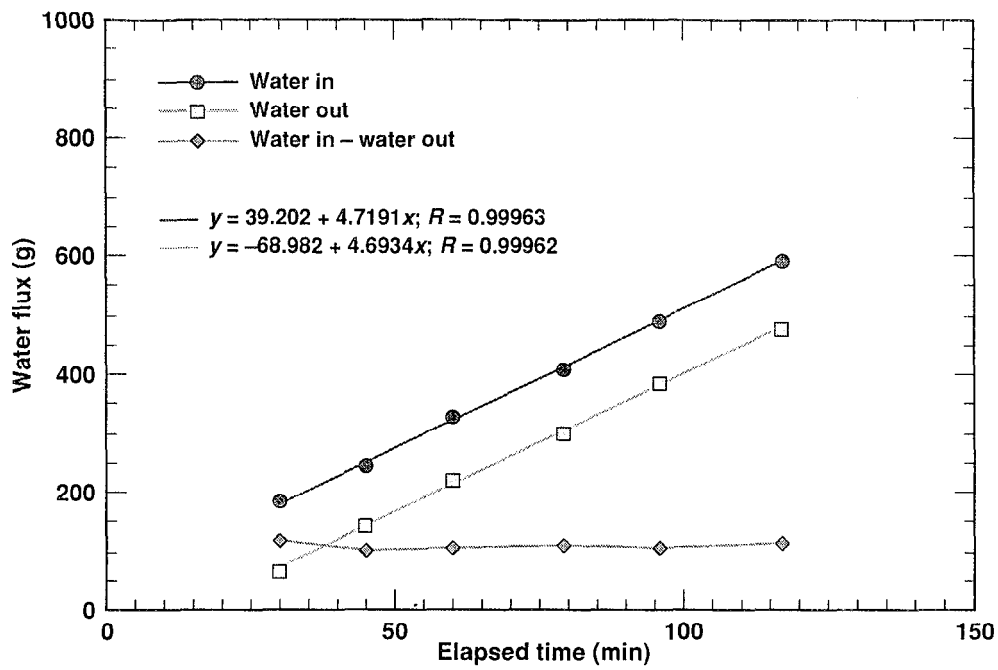


Figure 3. Fluid flow into the specimen during the initial experimental run

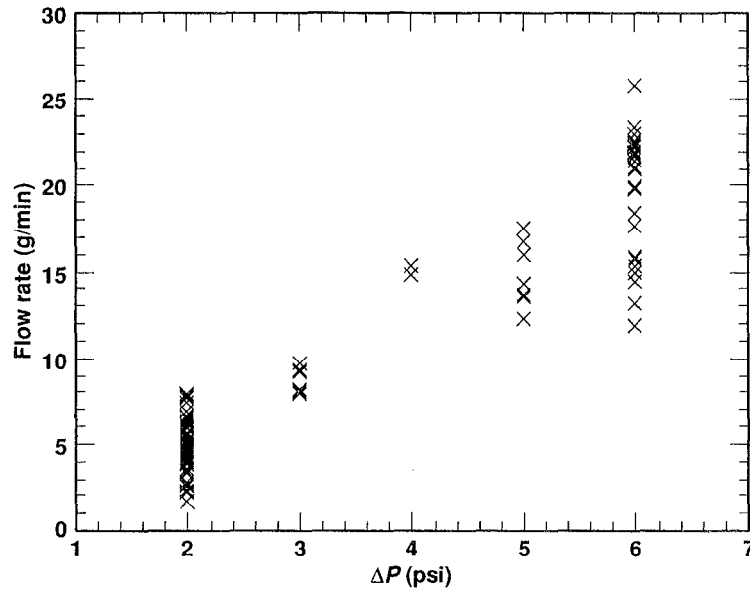


Figure 4. Flow rate versus pressure under various axial stress and temperature conditions

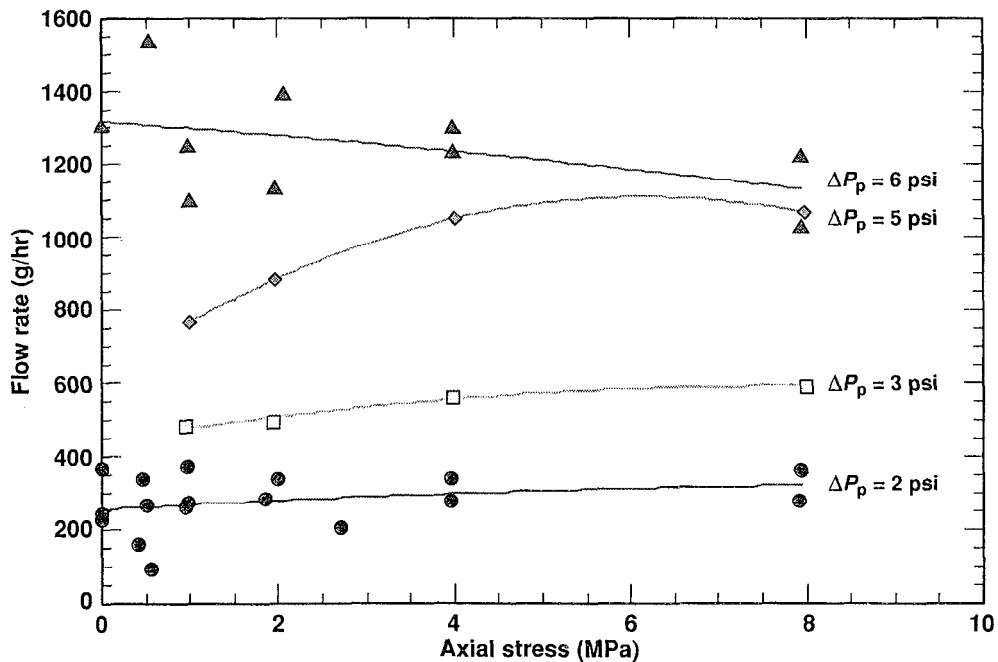


Figure 5. Water flow rate versus axial stress (lines are drawn only as an aid to the eye)

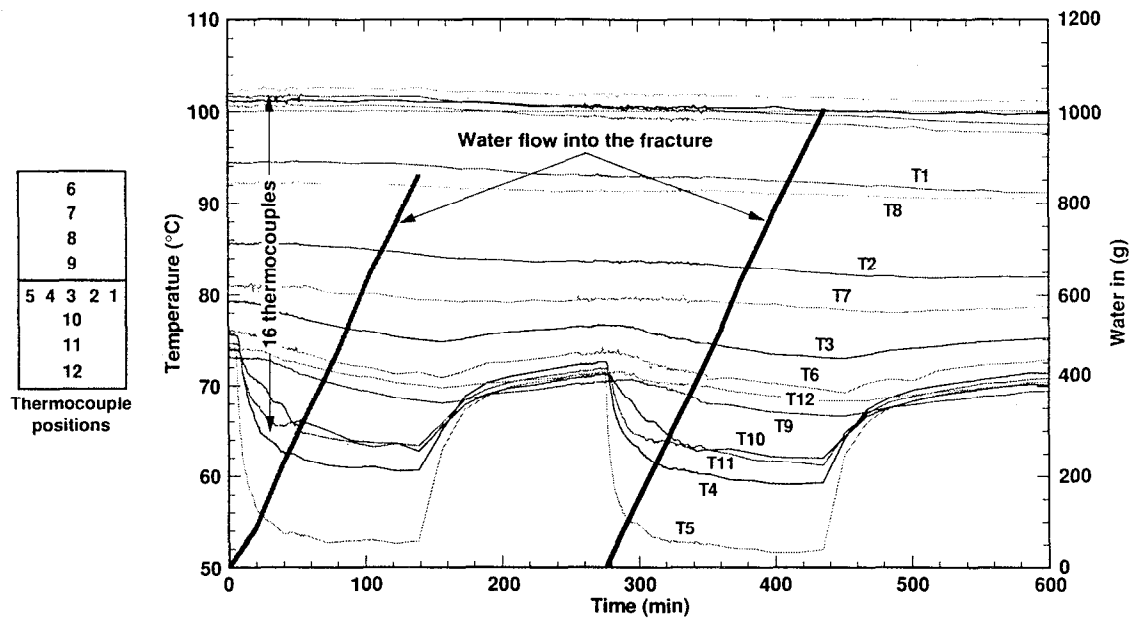


Figure 6. Temperature and cumulative water flow
Temperatures for the thermocouples in the rock are labeled T1–T12; those for thermocouples affixed to the copper heat-transfer plates on the top and bottom block surfaces are unlabelled. Water inflow for two periods is also shown.

Water flow rate is independent of mean fracture aperture, as parameterized through axial stress, owing to the intersection of rock porosity with the uncorrelated fracture surfaces.

3.4 Effect of fluid flow on the temperature field

A remarkable effect on the temperature field in the rock owing to fluid flow is shown in Figure 6. Initial conditions are no water flow and constant temperature at each thermocouple. Commencement of water flow from the room temperature reservoir brought a rapid drop in temperature for several thermocouples, but the effect was not monotonic with distance from

the fracture surface. Certain thermocouples near the fracture registered small or no changes in temperature, whereas some farther away registered quite large changes. Cessation of water flow followed a similar pattern: neither the order nor the magnitude of the thermocouple responses were strictly correlated with distance to the fracture.

The temperature data were fit to the solution for the 1-D heat-flow equation for a semi-infinite solid at uniform initial temperature T_0 and a constant boundary temperature T_B (Carslaw & Jaeger 1986):

$$T = T_B + (T_0 - T_B) \operatorname{erf} [z/(2\sqrt{\kappa t})] ; z \geq 0, t \geq 0. \quad (1)$$

Initial temperature T_0 and fracture distance z are

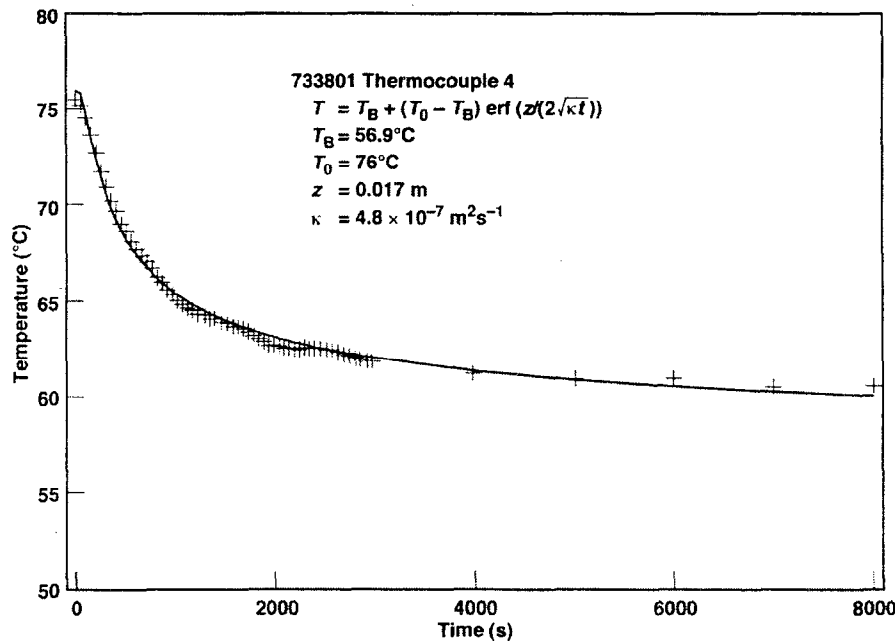


Figure 7. Temperature fit to the heat-flow equation for a semi-infinite solid with a known initial temperature and a constant temperature boundary

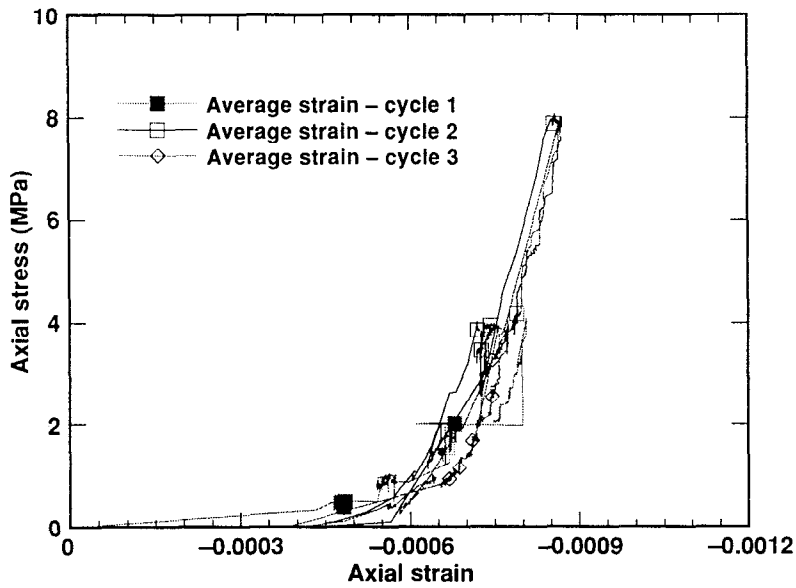


Figure 8. Average stress-strain curves for long baseline transducers over three loading cycles

fixed; water temperature in the fracture T_B and thermal diffusivity κ are fitting parameters. The total heat capacity of the water, calculated from the flow rate and time, is adequate to form a cold boundary condition at the fracture plane. Parameter fits for a typical flow-induced cooling episode are given in Table 1, and temperature fits for one thermocouple are shown in Figure 7.

Table 1. Parameter estimates, typical sample cooling episode

Thermocouple	z (m)	T_0 ($^{\circ}\text{C}$)	T_B ($^{\circ}\text{C}$)	κ ($\text{m}^2\text{s}^{-1} \times 10^{-6}$)
3	0.017	79	69.4	.03
4	0.017	76	56.9	.48
5	0.016	74	49.9	1.2
6	0.236	76	67.2	8.8
9	0.019	73	60.4	.03
10	0.082	74	58.0	2.6
11	0.146	74.5	61.0	25
12	0.214	74	65.3	4.8

3.5 Deformation

Axial strain, averaged over the four long-baseline transducers, shows the initial softness of the rock, followed by a stiffening to almost a linear response above an axial stress of about 4 MPa (Figure 8).

Table 2 lists estimates of effective elastic modulus for the initial loading cycle. The 2.8 GPa value at low axial stress is consistent with previous results on tuff blocks of similar size (Blair & Berge 1996) and is considerably lower than moduli typically found in laboratory tests on small cores, which lack large fractures and vugs. The rise in Young's modulus with axial stress reflects the closure of fractures.

Table 2. Young's modulus

Axial Stress (MPa)	Young's Modulus (GPa)
0-1	2.8
1-4	17
4-8	40

The displacements across both the rock matrix and the vugs were too small in this experiment to provide a reliable value for Poisson's ratio.

4 DISCUSSION

Two results of this experiment are of exceptional importance in the coupled THM phenomenology of fluid flow in YM. The first is the clear independence of fluid flow on stress normal to the fracture. The second is the overriding effect of heat flow along heat pipes formed by fluid-filled porosity.

4.1 Flow through fractures with uncorrelated surfaces

Application of 14 MPa of axial stress caused the fracture aperture to close by about 0.04 cm with no measurable change in flow rate. This observation was unexpected, but visual examination of the fracture surfaces and the surface profilometry data provide an explanation. The fracture surfaces were not well correlated in this experiment, so even at the highest applied axial stress, the load was carried by only a small fraction of the asperities. This left channels of connected porosity with cross-sectional areas on the order of 1 mm^2 through which water could flow. Surface profilometry measurements of the fracture plane, which was ground flat to better than .025 mm, preclude large (cm-scale) wavelength deviations from flatness, but the short (mm-scale) wavelength variation from flat parallel planes is pervasive and independent of normal stress. The flow paths through the porosity intersected by the fracture are built into the fracture and are independent of normal stress, so that a fluid-conduction path exists independent of the mean fracture surface displacement. Connectivity

depends on the total porosity and the pore size and shape distribution.

This effect is easily visualized by considering two parallel planes through a porous medium. Each plane contains “holes” representing the intersection of the plane with voids. Upon overlaying the planes, the union of the voids represents fluid-conduction paths. Above a percolation limit defined by the total porosity and its mean aspect ratio, a fracture surface formed by these two planes contains conduction paths that remain open, even at large normal stresses. The total flow is a sum of the flows through the porosity intersected by the fracture and the normal displacement of the mean fracture surfaces, so the fracture permeability never decreases to the matrix permeability. This phenomenology is not expected to be true for fractures having well-correlated surfaces, for which normal compressive stresses should simply reassemble the fracture and result in a porosity connectivity identical to the unfractured state.

The artificial fracture surfaces are uncorrelated in our experiment because about 6 mm of rock was removed by grinding. Fracture surfaces become uncorrelated in situ from shearing or time-dependent effects, such as chemical deposition or asperity erosion. Shear displacements on the order of the pore spacing can create connected flow paths that allow residual flow, regardless of the applied normal stress. This residual flow may be significantly higher than the flow through the unfractured matrix, because a larger fraction of the matrix porosity is connected. This process should be particularly important for rocks that have well-developed porosity texture or fabric. The texture defines a plane of minimum matrix area and, therefore, a weakness plane for shear failure. The geometry of shear failure in this plane results in two effects which enhance flow through the fracture. First, the density of the porosity intersecting a random plane in the host rock is highest in this failure plane. This provides the lowest impedance flow path of any direction. Second, the preferred alignment of high aspect ratio porosity results in a preferred flow direction within the fracture plane. We see this effect in our experiment, in which the larger pores have an aspect ratio generally greater than 5:1 and are preferentially aligned east–west. Figure 2 reflects this anisotropy in the dominant east–west flow volume through channels E5 and W6.

Computer models that employ a permeability based on a cubic flow law with an effective fracture separation may overestimate the effectiveness of mechanical or thermal loading in reducing flow through fractures if the opposing fracture surfaces are poorly correlated. Accounting for this “residual” permeability is particularly important if the model problem includes shear displacements of the fracture surfaces. For porous rocks, such as Topopah Spring tuff having macroscopic porosity greater than 10%

or so, the bulk of the fracture flow may occur along channels of connected porosity over a range of normal stress. Modeling the fracture permeability as a constant equal to the matrix permeability plus that owing to the normal displacement of the fracture surfaces misses any enhanced flow through the porosity connected along uncorrelated fracture surfaces. Even if the model retains a residual effective displacement to account for the shear displacement, the contribution of the porosity intersecting the fracture is lost. Of course, in lumped parameter models, all of this phenomenology is captured in a single number based on direct observation or by adjusting the parameter. At issue here is modeling the permeability of a sheared fracture knowing only the root-mean-square roughness of the fracture surface and the morphology of the matrix porosity.

4.2 Heat transfer through connected porosity

The second interesting observation from this intermediate-scale experiment concerns the effect of fluid flow on the temperature field in the block. As noted above, neither the order nor the magnitude of the thermocouple responses were strictly correlated with distance to the fracture. In addition, thermal diffusivities estimated from some of the heat-flow equation fits are much higher than expected. Thermal diffusivity, $\kappa = K/(\rho c)$, is the ratio of thermal conductivity K to the product of density ρ and specific heat c . Typical values for dry Topopah Spring tuff are $K = 1.5 \text{ W/m}\cdot\text{K}$ and $\rho c = 2 \text{ J/cm}^3\cdot\text{K}$ (DOE 1990), which yield $\kappa = 0.75 \times 10^{-6} \text{ m}^2/\text{s}$. Parameter fits for Thermocouples 6 and 11 (Table 1) indicate apparent thermal diffusivities 10 to 30 times higher.

These observations may be accounted for if fluid-filled fractures serve as rapid heat-transfer pathways within the rock. This “heat pipe” effect owes to advective heat transport by water in connected porosity and in fractures between the thermal boundary (the artificial fracture) and the thermocouples. A similar effect was observed in the field during the LBT (Blair & Lin 1997). The notion of high thermal conductance provided by a water-saturated path in a rock with low saturation is not new. However, the ability to characterize it in a controlled environment on the 0.5-m scale offers some useful guidance for computer modeling. Because of the heat pipe effect, local temperatures may depart considerably from average temperatures calculated based on matrix thermal conductivities. As chemical reactions depend upon local rather than average temperatures, computer models need to account for the heat pipe effect to model THM-coupled chemical reactions accurately in the repository NFE.

4.3 Anisotropy of mechanical properties

The stress-strain data from these intermediate-scale experiments reveal a marked anisotropy in Young's modulus. In previous work (Blair & Berge 1996), a Topopah Spring tuff sample was loaded normal to the rock fabric, yielding effective Young's moduli between 5 and 30 GPa. In the present experiment, the tuff block was loaded parallel to the rock fabric, yielding a higher effective Young's modulus of about 40 GPa for axial stresses above 4 MPa. Taking 15–20 GPa as a rough average effective modulus, yields an anisotropy on the order of 50%, significant for modeling the TM response of the NFE.

An axial stress of about 0.5 MPa was sufficient to close the artificial fracture mechanically. Thus, the "aperture" of the fracture, defined as the separation of the planes describing the average asperity height, does not change significantly with axial stress. This is consistent with the observation that fluid flow is independent of axial stress (i.e. fracture aperture). We conclude that an uncorrelated fracture can have a stiffness similar to the host rock and still can form a low-impedance flow path for fluids; fracture conductance remains large when the fracture closes.

5 SUMMARY

These results have significant implications for modeling coupled THM processes in the near-field environment. Shear displacement of fractures, whether from mining, from mechanical relaxation, or in response to thermal fields, will result in uncorrelated fracture surfaces. Fractures that intersect a porosity distribution above the percolation limit will form high-conductance paths for fluid into and out of the near-field environment, independent of the normal stress across the fracture. A lumped parameter parallel-plane model, in which fracture permeability approaches that of the host rock as normal stress increases, does not describe fracture flow correctly. Normal stresses on the fracture surface on the order of 1 MPa are sufficient to close the fracture mechanically, such that its stiffness is comparable to the host rock, but not hydraulically. Further, the fluid forms an advective and conductive thermal short circuit, compared to the host-rock thermal conductance.

REFERENCES

- Barton, C.A., M.D. Zoback & D. Moos 1995. Fluid flow along potentially active faults in crystalline rock. *Geology* 23(8):683–686.
- Blair, S.C. & P.A. Berge 1996. *Geomechanical properties of Topopah Spring tuff at the 0.5-m scale: preliminary results of compression tests at elevated temperature*. (UCRL-ID-125089) Livermore, CA: Lawrence Livermore National Laboratory.
- Blair, S.C. & M.S. Costantino 1997. *Preliminary results of a coupled fracture-flow test at the 0.5-m scale*. (UCRL-ID-129731) Livermore, CA: Lawrence Livermore National Laboratory.
- Blair, S.C. & W. Lin 1997. *Thermal-mechanical behavior of a heated 3-m block of fractured tuff*. (UCRL-JC-128350) Livermore, CA: Lawrence Livermore National Laboratory.
- Blair, S.C. & M.S. Costantino 1998. Anisotropic behavior in 0.5-m scale blocks of Topopah Spring tuff. In *Proceedings of the eighth international conference on high-level radioactive waste management conference*. p. 60. La Grange Park, IL: American Nuclear Society. (Also UCRL-JC-128800, Lawrence Livermore National Laboratory)
- Carslaw, H.S. & J.C. Jaeger 1986. *Conduction of heat in solids*. (2nd edition) Oxford, UK: Clarendon Press.
- Costantino, M.S., S.R. Carlson & S.C. Blair 1998. *Results of a coupled fracture-flow test at the 0.5-m scale*. (UCRL-ID-131493) Livermore, CA: Lawrence Livermore National Laboratory.
- DOE 1990. *Yucca Mountain Project reference information base, version 4*. (YMP/CC-0002) Las Vegas, NV: Yucca Mountain Site Characterization Project Office, U.S. Department of Energy.
- Hardin, E.L., S.C. Blair, T.A. Buscheck, D.A. Chesnut, L.D. DeLoach, W.E. Glassley, J.W. Johnson, R.B. Knapp, K. Lee, A. Meike, K. Myers, J.J. Nitao, C.E. Palmer, L.L. Rogers, N.D. Rosenberg, B.E. Viani, H.F. Wang, C. Wittwer & T.J. Wolery 1998. *Near-field/altered-zone models report*. (UCRL-ID-129179) Livermore, CA: Lawrence Livermore National Laboratory.
- Keller, K. & B.P. Bonner 1985. Automatic, digital system for profiling rough surfaces. *Rev. Sci. Instrum.* 56:330–331.
- Lin, W., D.G. Wilder, J.A. Blink, S.C. Blair, T.A. Buscheck, W.E. Glassley, K. Lee, M.W. Owens & J.J. Roberts 1995. A heated large block test for high level nuclear waste management. In *proceedings from Second international conference on mechanics of jointed and faulted rock: MJFR-2*. Vienna, Austria: April 10–14, 1995. (Also UCRL-JC-116418, Lawrence Livermore National Laboratory, Livermore, CA)
- Nitao, J.J., T.A. Buscheck & D.A. Chestnut 1993. Implications of episodic nonequilibrium fracture-matrix flow on repository performance. *Nucl. Technol.* 104:385–402
- Richards, L.A. 1931. Capillary conduction of liquids through porous mediums. *Physics* 1:318–333.
- Taylor, E.C. 1997. *Technical progress in the Yucca Mountain Project*. February 1997. (internal report to M&O contractor organizations)

Work performed under the auspices of the U.S. Department of Energy by the Lawrence Livermore National Laboratory under Contract W-7405-Eng-48.